PERGAMON Computers and Mathematics with Applications 41 (2001) 307–318

An International Journal
computers & mathematics
with applications

www.elsevier.nl/locate/camwa

Nonreflecting Boundary Condition for the Helmholtz Equation

A. S. DEAKIN AND H. RASMUSSEN
Department of Applied Mathematics
University of Western Ontario
London, Ontario, Canada, N6A 5B7

(Received August 1999; revised and accepted July 2000)

Abstract—To solve the Helmholtz equation in an infinite three-dimensional domain a spherical artificial boundary is introduced to restrict the computational domain Ω. To determine the nonreflecting boundary condition on $\partial\Omega$, we start with a finite number of spherical harmonics for the Helmholtz equation. With a precise choice of (primary) nodes on the sphere, the theorem on Gauss-Jordan quadrature establishes the discrete orthogonality of the spherical harmonics when summed over these nodes. An approximate nonreflecting boundary condition for the Helmholtz equation follows readily upon solving the exterior Dirichlet problem. The accuracy of the boundary condition is determined using a point source, and the computational results are presented for the scattering of a wave from a sphere.

Keywords—Exact boundary conditions, Acoustic scattering.

1. INTRODUCTION

We consider, in three space dimensions, special cases of the boundary value problem involving the Helmholtz equation

$$\nabla^2 u(x) + k^2 u(x) + f(x) = 0, \qquad x \in D, \tag{1}$$

$$\lim_{r\to\infty} r(u_r - iku) = 0, \qquad r = |x|, \tag{2}$$

$$u = g(x), \quad x \in \Gamma_g, \qquad \text{and} \qquad \frac{\partial u}{\partial n} = h(x), \quad x \in \Gamma_h, \tag{3}$$

where D is the infinite exterior domain to the boundary $\Gamma = \Gamma_h \cup \Gamma_g$, n refers to the exterior normal, and (2) is the radiation condition that is imposed at infinity. Problems of this type are important in the scattering of acoustic waves from a three-dimensional object.

To determine the numerical solution in an infinite domain, a spherical artificial boundary B of radius a is chosen so that the exterior Dirichlet problem can be solved analytically. In the infinite region exterior to B, we assume that for $|x| > a$

$$\nabla^2 u(x) + k^2 u(x) = 0, \tag{4}$$

This research was supported by NSERC of Canada.

0898-1221/01/$ - see front matter Typeset by AMS-TEX
PII: S0898-1221(00)00275-3

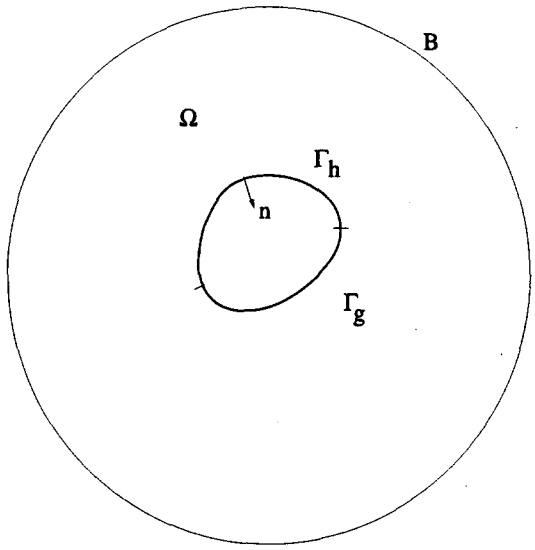

Figure 1. A typical configuration where the artificial boundary B is a sphere of radius a and Ω is the computational zone. Dirichlet and Neumann conditions are given on Γ_g and Γ_h, respectively.

where k is a constant. The computational zone Ω is restricted to the region between Γ and B (see Figure 1). Our concern in this paper, is the nonreflecting boundary condition that is imposed on B.

In this paper, we start with the Gauss-Jacobi quadrature formulas [1] to establish the orthogonality properties of the spherical harmonics when summed over a special set of nodes that we refer to as primary nodes. Then the exterior Dirichlet problem for the Helmholtz equation (2),(4) is solved in the region exterior to B for a finite number of eigenfunctions (see (6)). The boundary condition for the Helmholtz equation (Section 3) is expressed as a sum over the primary nodes on B. Our approach differs from the one used by Keller and Givoli [2], where the boundary condition is summed over all the nodes on B. The number of nonzero coefficients in the system of linear equations to be solved is much greater in the approach in [2] than in our approach. The only error in our boundary condition arises from the truncation of the series of eigenfunctions; whereas, the numerical evaluation of the Fourier integrals is required in [2].

The accuracy of our boundary condition is illustrated in Section 4, where we consider a point source in Ω and we determine the relative error of the normal derivative on B. In Section 5, we present the numerical aspects of our boundary condition for the Helmholtz equation using the finite difference method in the computational domain. We compute the solution of the boundary value problem for the scattering of a wave from a sphere where the incident wave is generated by a unit point source. We summarize our results in Section 6.

Based on our experience in applying nonreflecting boundary conditions to potential problems in two dimensions [3] and in a three-dimensional region between two planes [4], nonreflecting boundary conditions lead to accurate solutions.

2. FORMULATION

We discuss the numerical aspects of our boundary condition in Section 5, where we distinguish between the primary and secondary nodes on the spherical artificial boundary B of radius a. In spherical coordinates $x = (r, \theta, \phi)$, where $0 \leq \theta \leq \pi$ and $0 \leq \phi < 2\pi$, we define the primary nodes as $x_{pq} = (a, \theta_p, \phi_q)$, where $\phi_q = (q-1)2\pi/M$ $(q = 1, \ldots, M)$, and for reasons to be stated shortly, θ_p $(p = 1, \ldots, N)$ are the roots of the Legendre polynomial $P_N(\cos\theta) = 0$. We denote this set of primary nodes $\{x_{pq}\}$ by η_p. Numerical methods require that nodes be defined in the computational zone and on B, and we refer to these nodes on B as secondary nodes. In our

case, using the finite difference method, we select a regular set of secondary nodes on B denoted by η_s. The two sets η_s and η_p have the following properties: there are few nodes in common, the number of nodes in η_s can be much larger than the number of nodes in η_p, and the sparcity of the set of equations to be solved for u is improved by minimizing the number of nodes in η_p such that the desired accuracy is obtained.

The boundary condition for the Helmholtz equation is determined from the solution of the exterior Dirichlet problem for $|x| > a$. The general eigenfunction expansion that satisfies the radiation condition at infinity is

$$u(x) = \sum_{n=0}^{\infty} \sum_{m=-n}^{n} B_{nm} \frac{H^{(1)}_{n+1/2}(kr) r^{-1/2}}{H^{(1)}_{n+1/2}(ka) a^{-1/2}} Y_n^m(\theta, \phi), \tag{5}$$

where $H^{(1)}_{n+1/2}(kr)$ is the Hankel function of the first kind, the spherical harmonic $Y_n^m(\theta, \phi)$ is defined by $e^{im\phi} P_n^m(\cos\theta)$, and $P_n^m(\cos\theta)$ is the associated Legendre function. The Fourier coefficients B_{nm} are uniquely determined once $u(x)$ is given on the artificial boundary $|x| = a$. In the sequel, we formulate a discrete version of the Fourier coefficients.

LEMMA 1. *Suppose that the solution to (2),(4) is a linear combination of a finite number of spherical harmonics* $Y_n^m(\theta, \phi)$,

$$u_N(r, \theta, \phi) = \sum_{n=0}^{N-1} \sum_{m=-n}^{n} B_{nm} \frac{H^{(1)}_{n+1/2}(kr) r^{-1/2}}{H^{(1)}_{n+1/2}(ka) a^{-1/2}} Y_n^m(\theta, \phi). \tag{6}$$

Then, given u_N *at the primary nodes, the* N^2 *Fourier coefficients*

$$B_{nm} = (-1)^m \frac{2n+1}{2M} \sum_{p,q} \lambda(x_{pq}) Y_n^{-m}(\theta_p, \phi_q) u_N(x_{pq}) \tag{7}$$

are uniquely determined by the discrete orthogonality properties

$$\sum_q e^{i(m'-m)\phi_q} = \delta_{m'm} M, \qquad |m' - m| < M \quad (M \geq 2N-1), \tag{8}$$

$$\int_{-1}^{1} P_n^m(\mu) P_{n'}^{-m}(\mu)\, d\mu = \sum_{p=1}^{N} \lambda(x_{pq}) P_n^m(\mu_p) P_{n'}^{-m}(\mu_p) = \delta_{n'n} \frac{2(-1)^m}{2n+1}, \tag{9}$$

where $\mu = \cos\theta$, $\mu_p = \cos\theta_p$ $(p = 1, \ldots, N)$ *are the zeros of the Legendre polynomial* $P_N(\mu)$, $\lambda(x_{pq})$ *is the Christoffel number associated with the zero* x_{pq}, *and* $\delta_{m'm}$ *is the Kronecker delta (see [1]).*

The proof readily follows by evaluating (6) at the primary nodes and applying the orthogonality properties to determine the coefficients B_{nm}. One expression for the coefficient $\lambda(x_{pq})$ is (see [1, p. 47])

$$\lambda(x_{pq}) = \frac{2}{N P_{N-1}(\mu_p) P'_N(\mu_p)} = \frac{2(1-\mu_p^2)}{(N P_{N-1}(\mu_p))^2}. \tag{10}$$

Although $\lambda(x_{pq})$ is independent of q, this notation is convenient for later use. Note that the orthogonality property (8) is unaffected if $\phi_q = c + (q-1)2\pi/M$, where c is any arbitrary number. Thus, without loss of generality, we can take $c = 0$, since a rotation of the coordinate system about the z-axis would remove this term. In addition, if $M < 2N-1$, then the sum in (8) over q is equal to M whenever $m' - m = (\text{Integer}) * M$.

The expression for $u_N(r,\theta,\phi)$ is readily obtained by substituting (7) into (6) and, by using the addition theorem [5],

$$P_n\left(\cos\psi\left(x,x_{pq}\right)\right)=\sum_{m=-n}^{n}(-1)^m Y_n^m\left(\theta,\phi\right)Y_n^{-m}\left(\theta_p,\phi_q\right), \tag{11}$$

$$\cos\left(\psi\left(x,x_{pq}\right)\right)=\sin\left(\theta_p\right)\sin\left(\theta\right)\cos\left(\phi_q-\phi\right)+\cos\left(\theta_p\right)\cos(\theta), \tag{12}$$

where $\psi(x,x_{pq})$ is the angle between the rays from the origin to the points $x=(a,\theta,\phi)$ and $x_{pq}=(a,\theta_p,\phi_q)$. Thus, (6) may be expressed as

$$u_N\left(r,\theta,\phi\right)=\sum_{p,q}\sum_{n=0}^{N-1}\frac{H_{n+1/2}^{(1)}(kr)r^{-1/2}}{H_{n+1/2}^{(1)}(ka)a^{-1/2}}\Lambda\left(x_{pq}\right)C_n\left(x,x_{pq}\right)u_N\left(x_{pq}\right), \tag{13}$$

$$C_n\left(x,x_{pq}\right)=P_n\left(\cos\psi\left(x,x_{pq}\right)\right)(2n+1), \tag{14}$$

where $\Lambda(x_{pq})=\lambda(x_{pq})/(2M)$ has the property that $\sum_{p,q}\Lambda(x_{pq})=1$.

In the sequel, it is convenient to replace the sum over the indices p and q in x_{pq} by the sum over the primary nodes α in the set $\eta_p=\{x_{pq}\mid p=1,\ldots,N;\ q=1,\ldots,M\}$.

3. BOUNDARY CONDITION FOR THE HELMHOLTZ EQUATION

The derivative $\frac{\partial u_N}{\partial r}$ at any point x on the boundary is derived from (13) by differentiating with respect to r.

THEOREM 1. *At any point x on the artificial boundary, u_N and $\frac{\partial}{\partial r}(ru_N)-ikru_N$ are a linear combination of u_N at the primary nodes*

$$u_N(x)=\sum_{\alpha\in\eta_p}\Lambda(\alpha)S_N(x,\alpha)u_N(\alpha), \tag{15}$$

$$\left(\frac{\partial}{\partial r}(ru_N)-ikru_N\right)(x)=\sum_{\alpha\in\eta_p}\sum_{n=1}^{N-1}\Lambda(\alpha)C_n(x,\alpha)G_n(ka)u_N(\alpha), \tag{16}$$

where

$$S_N(x,\alpha)=P_N'(\cos\psi(x,\alpha))+P_{N-1}'(\cos\psi(x,\alpha)), \tag{17}$$

$$G_n(z)=\sum_{j=1}^{n}\frac{z_{nj}}{z-z_{nj}}, \tag{18}$$

and z_{nj} are the zeros of $H_{n+1/2}^{(1)}(z)$.

To show these results, we set $r=a$ in (13) and then use Christoffel's first identity (34) in the Appendix to obtain (17) for $S_N(x,\alpha)$. For equation (16) involving the derivative, we differentiate (13) in r at $r=a$ and then we express the ratio of Hankel functions in another form. From the definitions

$$H_{n+1/2}^{(1)}(z)=\sqrt{\frac{2}{\pi z}}e^{i(z-(n+1)\pi/2)}F\left(n+1,-n;\frac{1}{2iz}\right), \tag{19}$$

$$F(n+1,-n;w)=\sum_{j=0}^{n}\frac{(n+j)!}{(n-j)!}\frac{(-w)^j}{j!}, \tag{20}$$

where F is the generalized hypergeometric function ${}_2F_0$ [5], we have

$$a\frac{\frac{\partial}{\partial a}\left(H^{(1)}_{n+1/2}(ka)a^{-1/2}\right)}{H^{(1)}_{n+1/2}(ka)a^{-1/2}} = ika - 1 + G_n(ka), \tag{21}$$

$$G_n(z) = \frac{z\frac{\partial}{\partial z}F(n+1,-n;1/(2iz))}{F(n+1,-n;1/(2iz))}. \tag{22}$$

The simplest way to compute $G_n(z)$ is to determine the zeros of $F(n+1,-n;1/(2iz))$ which are the zeros of $H^{(1)}_{n+1/2}(z)$. In the complex z-plane for each $n \geq 1$, there are n simple zeros $z_{nj} = a_{nj} - ib_{nj}$ $(j = 1,\ldots,n)$, where $b_{nj} \geq 1$, and these roots lie symmetrically with respect to the imaginary axis. Only for n odd is there a pure imaginary root. Furthermore, for any n and j, all roots z_{nj} are distinct [5,6]. For $n \leq 5$, the zeros are given by Hansen [7], and the asymptotic formula for the location of these roots for large n is given by Olver [8]. From (22), we have $G_n(z) = \sum_j z_{nj}/(z - z_{nj})$.

The boundary condition given by Keller and Givoli [2] can be readily derived from (15) and (16). Regarding $u_N(\alpha)$ as a parameter, we express $u_N(\alpha)$ (see (38) in the Appendix) in terms of an integral of $u_N(x)$ over B. Upon substituting this expression into (16) and using (33) and (38), we have the Dirichlet to Neumann map.

LEMMA 2. *Boundary conditions (15) and (16) are equivalent to*

$$\left(\frac{\partial}{\partial r}(ru_N) - ikru_N\right)(x) = \frac{1}{4\pi}\sum_{n=1}^{N-1}\int_0^{2\pi}\int_0^{\pi} C_n(x,x')G_n(ka)u_N(x')\sin(\theta')d\,\theta' d\,\phi', \tag{23}$$

where $C_n(x,x')$ is defined by (14) and $x' = (a,\theta',\phi')$.

This result agrees with the boundary condition of Keller and Givoli [2] if we let $N \to \infty$.

For $N = 1$ in (16), we define the expression on the right to be zero so that (16) becomes $\frac{\partial}{\partial r}(ru_N) - ik(ru_N) = 0$. Bayliss *et al.* [9] defined a sequence of boundary conditions for u. By applying their approach to ru instead of u, we have this first-order local boundary condition.

4. ACCURACY OF THE BOUNDARY CONDITION

Here, we determine the accuracy of our boundary condition by using a unit point source for which we know the solution. We take the solution of the Helmholtz equation to be

$$w(x) = \frac{e^{iks}}{4\pi s}, \qquad s^2 = a^2 + 1 - 2a\cos\theta, \tag{24}$$

where s is the distance between $x = (a,\theta,\phi)$ and the unit point source at $(1,0,0)$ on the z-axis inside B.

Owing to symmetry, the boundary condition (16) simplifies since $u_N(x_{pq})$ is independent of q. Using the orthogonality property (8), we have

$$\sum_q C_n(x,x_{pq})u_N(x_{pq}) = M(2n+1)P_n(\mu)P_n(\mu_p)u_N(x_{p1}). \tag{25}$$

From (16), the boundary condition becomes

$$\frac{\partial u_N}{\partial r}(x) = \left(ik - \frac{1}{a}\right)u_N(x) + \frac{1}{a}\sum_p \kappa_p(\mu,ka)u_N(x_{p1}), \tag{26}$$

where

$$\kappa_p(\mu,ka) = \sum_{n=1}^{N-1}\frac{2n+1}{2}\lambda(x_{p1})P_n(\mu)P_n(\mu_p)G_n(ka). \tag{27}$$

To measure the accuracy of the boundary condition (26), we compare the normal derivative w_r on B to the derivative $\frac{\partial u_N}{\partial r}$ determined by the boundary condition (26) in which $u_N(x) = w(x)$. To this end, we computed, using Maple V Release 5, the maximum relative error $E(a, N, k)$ on B,

$$E(a, N, k) = \max_{x \in B} \left| \frac{\frac{\partial u_N(x)}{\partial r} - w_r(x)}{w_r(x)} \right|. \tag{28}$$

In Figure 2, $\log_{10} E(a, N, k)$, as a function of N, is graphed for three values of the parameter k where $a = 2$. In this figure, the relative error peaks at N near k, and thereafter, approaches a straight line. Clearly, our approach does not work for k larger than about 20 for $a = 2$ since the coefficients in the boundary condition become increasingly more difficult to compute with increasing N. For a fixed k, the error decreases as a increases, and the curves have the same general features: the graphs are displaced downward and the slope for large N increases.

We note that Figure 2 can be applied to the case where the scattering object is a sphere of radius b by scaling the variables. Let the unscaled variables be $\hat{r} = br$ and $\hat{k} = k/b$. The results in Figure 2 can now be expressed in terms of the unscaled variables where $2b$ is the radius of the artificial boundary and $\hat{k} = k/b$ is the corresponding wave number in the unscaled variables.

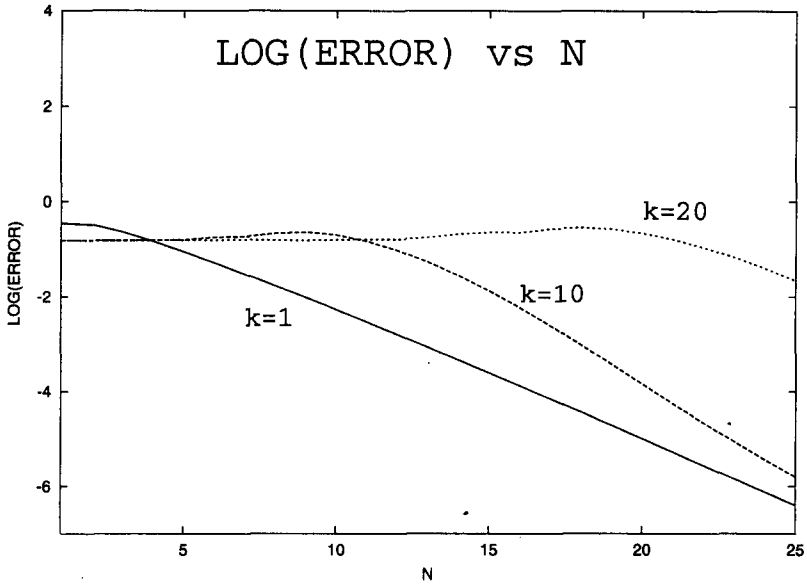

Figure 2. The semilog plot of LOG(ERROR) $= \log_{10} E$ vs. N is shown where E is the relative error (28). For $N = 1$, the kernel in (27) is defined to be zero. The three cases for $a = 2$ are $k = 1$, $k = 10$, and $k = 20$.

5. NUMERICAL PROCEDURE

In order to verify our procedure, we calculate the numerical solution for the scattering of a wave from a unit point source at $x' = (r', \theta', \phi')$ which is located outside the unit sphere centered at the origin. The solution, which vanishes on the unit sphere, is the Green's function (see [10, p. 360]). The incident wave is given by

$$u_i = \frac{e^{iks}}{s}, \qquad s^2 = r'^2 + r^2 - 2r'r\cos\psi\,(x, x')\,, \tag{29}$$

where s is the distance from the source point x' to any point $x = (r, \theta, \phi)$. From this incident wave, we formulate the boundary value problem for the scattered wave u, and it is this problem that we solve numerically and compare the results with the exact solution

$$u = \frac{\pi}{2i\sqrt{rr'}} \sum_{n=0}^{\infty} C_n(x, x') \frac{H^{(1)}_{n+1/2}(kr) H^{(1)}_{n+1/2}(kr') J_{n+1/2}(k)}{H^{(1)}_{n+1/2}(k)}, \tag{30}$$

where $u = -u_i$ on the sphere $r = 1$.

We define a regular finite-difference grid by $u_{i,\ell,j} = u_N(r_i, \theta_\ell, \phi_j)$ with

$$r_i = 1 + \frac{i(a-1)}{n_r}, \qquad \theta_\ell = \frac{\ell\pi}{n_\theta}, \qquad \phi_j = \frac{(j-1)2\pi}{n_\phi}, \tag{31}$$

where n_r, n_θ, n_ϕ are integers. The secondary nodes on B are $x_{\ell j} = (a, \theta_\ell, \phi_j)$.

At $r = 1$, the boundary condition is $u = -u_i$ where u_i is defined by (29). Thus, the difference equations at $r_0 = 1$ are $u_{0,\ell,j} = -u_i(1, \theta_\ell, \phi_j)$. At the artificial boundary, the finite-difference form of the boundary condition (16) is more complicated and we use a second-order backward difference approximation.

The numerical procedure consists of replacing the Helmholtz equation in Ω, expressed in spherical coordinates, by a system of finite-difference equations obtained using second-order difference formulae. The difference approximations are standard except at the poles $\theta = 0$ and $\theta = \pi$. Let us consider a typical point $(r_i, 0, \phi_j)$ on the z-axis for some given i. At this point, we use a local Cartesian coordinate system and a form of the mean value property of the Helmholtz equation to obtain a finite-difference approximation in terms of the values of u along a small circle centered at our point and in the plane perpendicular to the z-axis. However, these points do not coincide with the original grid points so we must use a Taylor expansion to express u at these points in terms of $u_{i-1,\ell,j}$, $u_{i,\ell,j}$, and $u_{i+1,\ell,j}$ to second-order accuracy. A similar approach is carried out for the case $\theta = \pi$.

Since the primary nodes are regular in the ϕ variable, we select the regular secondary nodes such that the primary nodes are on some of the great circles on which we have the secondary nodes. Then, we express u at the primary nodes that are not secondary nodes as the linear interpolant $u(x_{pq}) = c_{pq}u(x^1_{pq}) + d_{pq}u(x^2_{pq})$ where x^i_{pq} are the two nearby secondary nodes on the same great circle as x_{pq}.

We now consider the sparcity of the system of equations to be solved for u at the nodes in Ω and the secondary nodes on B. This structure applies to the three types of boundary conditions that we consider on the artificial boundary. The first step is to express u at the primary nodes in the boundary condition in terms of u at the nearby secondary nodes. The equations have the form $\sum_{j=1}^{n_r} A_{ij}U_j = B_i$ $(1 \le i \le n_r)$, where A_{ij} is a square matrix. U_j are column vectors where the components of U_j are the values of u at the $(n_\theta - 1)n_\phi + 2$ nodes on the sphere of radius r_j. As a consequence of the discretisation of the Helmholtz equation, the diagonal and off-diagonal blocks of A_{ij} for $i < n_r$ are sparse and the remaining blocks are zero. However, in the last row, the block for $i = j = n_r$ is dense where the level of density depends on the particular boundary condition, the preceding two blocks are sparse, and the remaining blocks in the last row are zero. Finally, B_i is nonzero for $i = 1$ from the boundary condition on the sphere of radius 1, and the remaining blocks are zero.

Since the coefficient matrix of this linear system is very sparse, it is advantageous to use a sparse matrix solver and since the system is quite large, we decided to use an iterative solver. After studying the different sparse matrix solvers, we decided to use the PETSc package from Argonne National Laboratory. This package contains several iterative schemes with several preprocessors. After some experimentation we found the BICGSTAB (biconjugate gradient stabilized) method with an incomplete LU preprocessor with fill level of 3 was best suited for this problem. All computations were obtained using a Pentium running at 400 MHz with 256 Megabytes of RAM.

Many of the terms in the boundary conditions (16) can be computed using a CAS package—we used Maple V Release 5—and stored for future use. In this way, we computed the values of the zeros of $P_n(\mu)$ and $H_{n+1/2}(z)$ for all values of n required as well as the corresponding values for $\lambda(x_{pq})$.

We compare and contrast our approach with that of Keller and Givoli [2] by approximating (23), accurate to the second order. To do this, we partition the sphere of radius a into regular elements in which each element is centered about a secondary node. Thus, the boundary condition (23)

Table 1. These parameter settings for the nodes satisfy the condition that the diagonal of the largest element in the grid is approximately 0.20. The number of primary nodes is MN where, except in Figure 5, $M = n_\phi$. The number of linear equations to be solved varies from 15,000 to 60,000. The number of iterations in the sparse matrix solver varies from 5 to 10.

a	n_r	n_ϕ	n_θ
1.1	10	52	26
1.2	10	56	28
1.3	15	60	30
1.4	20	64	32
1.5	25	68	34

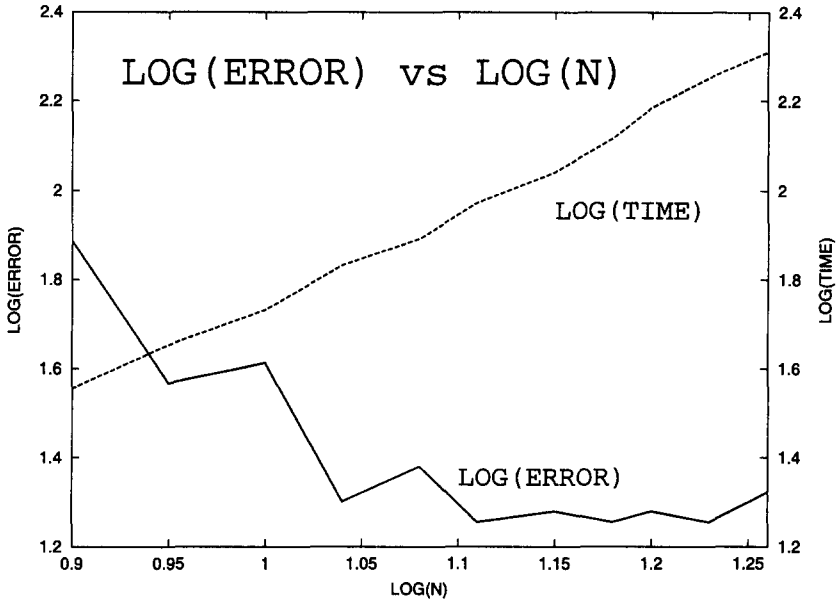

Figure 3. The plots LOG(TIME) and LOG(ERROR) as a function of LOG(N) are shown where LOG is the logarithm to base 10, ERROR = (relative error) $\times 10^4$, TIME is the cpu time in seconds, and N is the number of terms in the boundary condition (16). Parameter settings are given in Table 1, the source point is $(1.5, \pi/2, 0)$, and the radius of the artificial boundary is $a = 1.3$.

for Keller's method is approximated by

$$\left(\frac{\partial}{\partial r}(ru_N) - ikru_N\right)(x) = \sum_{\alpha\in\eta_s}\sum_{n=1}^{N-1} \Lambda(\alpha)C_n(x,\alpha)G_n(ka)u_N(\alpha), \tag{32}$$

where $\Lambda(\alpha) = \sin\theta(\alpha)\Delta\theta\Delta\phi/(4\pi)$ when α is not a polar node, and $\Lambda(\alpha) = \pi(\Delta\theta/2)^2/(4\pi)$ when α is a polar node. Equation (16) resembles (32) where $\sum_{\alpha\in\eta_s}\Lambda(\alpha) \approx 1$.

Our numerical results are presented in Figures 3–6, where LOG refers to the logarithm to base 10. The various parameters for the nodes are specified in Table 1. Note that the diagonal of the largest element of the grid in Ω is fixed at approximately 0.20. The maximum relative error in the computational zone Ω and B is defined as ERROR = $\max|(u_N - u)/u| \times 10^4$ where u_N is the numerical solution and u is the exact solution (30). In these figures, TIME is the CPU time in seconds, and the graph of LOG(TIME) is approximately a straight line so that the behaviour of TIME can be readily estimated in terms of the independent variable.

In Figure 3, the plot of LOG(ERROR) vs. LOG(N) is given as N varies from 8 to 18. For N in (8,9,10,11–18), ERROR has the corresponding value $(77, 37, 41, 21 \pm 3)$, respectively, where $a = 1.3$ and $r' = 1.5$. Essentially, for $N \geq 11$, ERROR is not affected by the boundary condition.

In Figure 4, LOG(ERROR) is plotted as a function of LOG(r'), where ERROR is computed in the same way as in Figure 3 and the radial distance r' of the unit point source varies from 1.1 to 1.9. As $r' \to 1+$, the ERROR increases rapidly since the exact solution is singular in the limit.

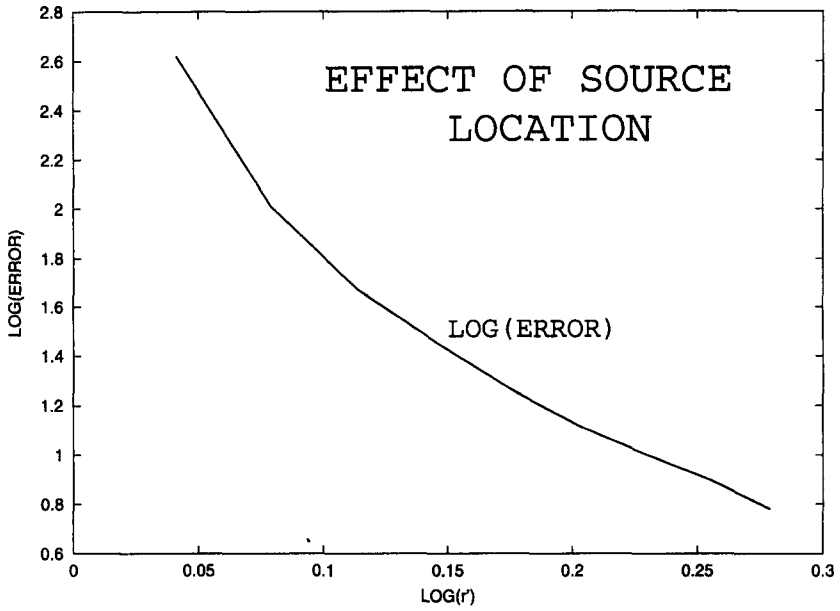

Figure 4. The plot of LOG(ERROR) (see Figure 3) as a function of LOG(r'), where the source is located at $(r', \pi/2, 0)$. The parameter settings are given in Table 1, $a = 1.3$, and $N = 15$.

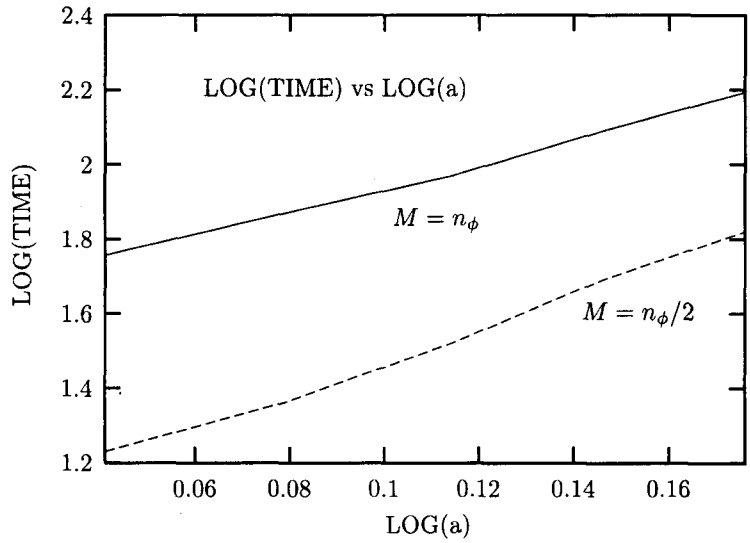

Figure 5. The plot LOG(TIME) vs. LOG(a) for two cases where $M = n_\phi$, $M = n_\phi/2$, and $N = 13$ where MN is the number of primary nodes. The parameter settings, except for M, are given in Table 1, and the source is at $(1.5, \pi/2, 0)$. In all cases, ERROR is less than 20.

In Figure 5, we show the effect of changing the number of primary nodes in the boundary condition (16). The number of secondary nodes on B is $(n_\theta - 1)n_\phi + 2$ and the number of primary nodes is MN where $N = 13$. The best value for M is approximately $2N - 1$ which is the lower limit for M in (8). The computational times are significantly affected by reducing the number of nonzero coefficients in the boundary condition. As in Figures 3 and 6, the graph of LOG(TIME) is approximately a straight line.

In Figure 6, we plot LOG(ERROR) and LOG(TIME) as a function of LOG(a) using Keller's method (see (32)). ERROR and TIME using the boundary condition (16) are much smaller. From Figure 3, for $N = 15$, $a = 1.3$, and $r' = 1.5$, we have for our approach ERROR = 18 and TIME = 130. The corresponding values for the Keller method are ERROR = 320 and TIME = 635. We used the same preconditioner and the same iterative procedure for both boundary conditions. It is possible that with another choice, Keller's method could be more efficient. In addition, a higher-order approximation than the second-order approximation of the integrals in (23) will improve the numerical accuracy of the boundary condition. Note that in (16), we use a second-order approximation to relate u at a primary node with u at the nearby secondary nodes.

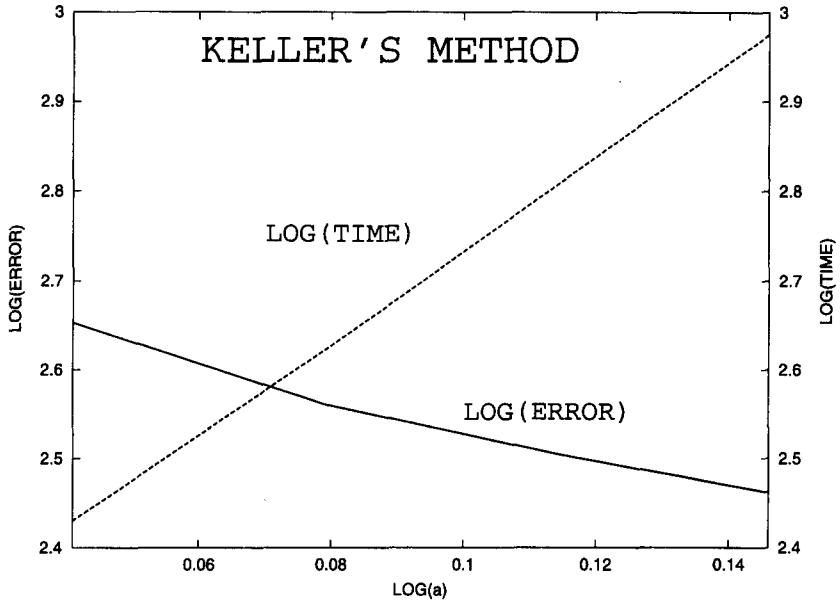

Figure 6. The plot of LOG(ERROR) (see Figure 3) and LOG(TIME) as a function of LOG(a), where the parameter settings are given in Table 1, $N = 15$, and the source is at $(1.5, \pi/2, 0)$.

Finally, we consider an alternative approach where condition (16) is applied at certain nodes and condition (15) is applied at the remaining nodes. To show this, we evaluate (15) at the primary nodes to obtain $\sum_{\alpha\in\eta_p}(\Lambda(\alpha)S_N(\beta,\alpha) - \delta_{\alpha,\beta})u_N(\alpha) = 0$ where $\beta \in \eta_p$. From (7), we conjecture that the rank of this coefficient matrix is $MN - N^2$. By computing the singular values of the coefficient matrix, we have $MN - N^2$ equations relating the MN unknowns $u_N(\alpha)$. We checked this conjecture by computing the singular values, using Maple V, for some small values for N and M. Consequently, in the case where the primary nodes are also secondary nodes, we conjecture that the derivative boundary condition (16) must be applied at a minimum of N^2 of the primary nodes and the boundary condition (15) is applied at the remaining nodes. Another simpler possibility would be to apply (16) at all of the primary nodes and then use (15) at the remaining secondary nodes.

In the example, we use to test this approach to the boundary condition, we apply (16) at all secondary nodes that are less than π/n_θ radians away from a primary node in the θ variable (about $2MN$ nodes), and at the remaining secondary nodes, we apply (15). In this case, since TIME and ERROR did not change significantly from those in Figure 3, they are not presented. Although a combination of (15) and (16) provide an efficient boundary condition, it is worth noting that more than 75% of the computational time is involved in solving the set of linear equations.

6. CONCLUSIONS

If only the first N^2 eigenfunctions (see (5)–(7)) are present in the solution, the boundary condition (16) is exact. In general, however, the choice of N in the boundary condition is based on the number of significant eigenfunctions, that are expected, in the solution on the artificial boundary. Effectively, this choice defines the MN primary nodes if we select M near the minimum value of $2N-1$. From a computational point of view, the execution time increases as the number of primary nodes increases. The next step involves the size of the mesh in the computational zone which includes the secondary nodes on B, and this choice is based on the expected rate of change of the solution. In Figures 3–6, we illustrate the relative error and the computational time for various settings of the parameters for the scattering of waves from the unit sphere where the waves are generated at a unit point source.

The numerical solution of the wave equation for large k has two difficulties. For fixed a, the mesh size in the computational zone must decrease with increasing k, and the number of terms in the boundary condition must increase. From Figure 2, for k larger than approximately 20 and $a = 2$, the number of terms N in the boundary condition that are required for a reasonably accurate solution becomes large, and consequently, the computational complexity of the boundary condition increases sharply. With fixed k and a specified accuracy, the radius of the artificial boundary can be increased so that fewer terms in the boundary condition are required; however, the number of nodes in Ω increases so that the computational time also increases.

For an accurate numerical solution using the standard boundary condition (23), higher-order approximations of the integrals are required on the artificial boundary; or, the number of secondary nodes must be increased to improve the accuracy of the boundary condition. The difference in accuracy, using the boundary conditions (16) and (23), reminds us of the increase in accuracy between Gaussian integration and standard integration techniques.

APPENDIX

PROPERTIES OF $C_n(x,\alpha)$

PROPERTY I. The basic property for the symmetric coefficients $C_n(x,\alpha)$ is $\sum_{\alpha\in\eta_p} \Lambda(\alpha)C_n(x,\alpha) = \delta_{n0}$ which is proved from (8)–(14). Hence, from (15), if $u_N(\alpha)$ is a constant then $u_N(x)$ is equal to this constant at any point on B. In addition, as expected, the formula for derivative (16) on B simplifies where the expression on the right of (16) is zero.

PROPERTY II. To determine the sum

$$S_N(x,\alpha) = \sum_{n=0}^{N-1} C_n(x,\alpha) \tag{33}$$

in (17), we start with the Christoffel's first identity

$$(\rho-\xi)\sum_{m=0}^{n}(2m+1)P_m(\xi)P_m(\rho) = (n+1)[P_{n+1}(\rho)P_n(\xi) - P_n(\rho)P_{n+1}(\xi)]. \tag{34}$$

Upon setting $\xi = 1$ and $\rho = \cos\psi$ where $\psi = \psi(x,\alpha)$, we have

$$S_N(x,\alpha) = \begin{cases} N\dfrac{P_N(\cos\psi) - P_{N-1}(\cos\psi)}{\cos\psi - 1}, & \psi \neq 0, \\ N^2, & \psi = 0. \end{cases} \tag{35}$$

Using the recurrence relations for Legendre polynomials, this expression for S_N can be written in form (17).

PROPERTY III. The orthogonality property for $C_n(x,\alpha)$ is

$$\frac{1}{4\pi}\int_0^{2\pi}\int_0^{\pi} C_n(x,\alpha)C_{n'}(x,\beta)\sin(\theta)\,d\theta\,d\phi = \delta_{nn'}C_n(\alpha,\beta), \qquad \alpha,\beta\in\eta_p. \tag{36}$$

The proof follows directly from (11),(14) as well as the orthogonality property of the spherical harmonics

$$\int_0^{2\pi}\int_0^{\pi} Y_n^{-m}(\theta,\phi)Y_{n'}^{m'}(\theta,\phi)\sin(\theta)\,d\theta\,d\phi = \frac{4\pi(-1)^m}{2n+1}\delta_{nn'}\delta_{mm'}. \tag{37}$$

PROPERTY IV. From (15), we express u_N at the primary nodes in terms of an integral of u_N over B

$$u_N(\alpha) = \frac{1}{4\pi}\int_0^{2\pi}\int_0^{\pi} S_N(x,\alpha)u_N(x)\sin(\theta)\,d\theta\,d\phi. \tag{38}$$

To prove this result, we multiply (15) by $\sum_{n'=0}^{N-1} C_{n'}(x,\beta)$ and integrate over B. Using (33) and the previous identity (36), the result follows directly.

PROPERTY V. The discrete orthogonality property is

$$\sum_{\alpha\in\eta_p} C_n(x,\alpha)C_{n'}(x',\alpha)\Lambda(\alpha) = C_n(x,x')\delta_{nn'}, \tag{39}$$

where $x,x'\in B$. This identity follows readily from (11)–(14), and the discrete orthogonality properties (8) and (9).

REFERENCES

1. G. Szegö, *Orthogonal Polynomials, Vol. 23*, AMS Colloq., New York, (1959).
2. J.B. Keller and D. Givoli, Exact non-reflecting boundary conditions, *J. Comput. Phys.* **82**, 172–192, (1989).
3. A.S. Deakin and J.R. Dryden, Numerically derived boundary conditions on artificial boundaries, *J. Comp. Appl. Math.* **58**, 1–16, (1995).
4. A.S. Deakin and H. Rasmussen, Sparse boundary conditions on artificial boundaries for three-dimensional potential problems, *J. Comput. Phys.* **129**, 111–120, (1996).
5. A. Erdélyi *et al.*, Higher transcendental functions, In *Bateman Manuscript Project, Volumes I and II*, R.E. Kreiger, Melbourne, FL, (1985).
6. M. Abramowitz and I.A. Stegun, *Handbook of Mathematical Physics*, Dover, New York, (1965).
7. T.B. Hansen, Formulation of spherical near-field scanning in the time domain, In *Computational Wave Propagation, Volume 86*, IMA, (Edited by B. Engquist *et al.*), pp. 45–74, Springer, New York, (1997).
8. F.W.J. Olver, The asymptotic expansion of Bessel functions of large order, *Phil. Trans. Roy. Soc. London Ser. A* **247**, 328–368, (1954).
9. A. Bayliss, M. Gunzburger and E. Turkel, Boundary conditions for numerical solution of elliptic equations in exterior regions, *SIAM J. Appl. Math.* **42**, 430–451, (1982).
10. G.F.D. Duff and D. Naylor, *Differential Equations of Applied Mathematics*, J. Wiley, New York, (1966).